



LIGS measurements in the nozzle reservoir of a free-piston shock tunnel

P. Altenhöfer¹ · T. Sander¹ · F. Koroll¹ · Ch. Mundt¹

Received: 2 June 2017 / Revised: 6 October 2017 / Accepted: 18 January 2018 / Published online: 10 February 2018
© Springer-Verlag GmbH Germany, part of Springer Nature 2018

Abstract

Free-piston shock tunnels are ground-based test facilities allowing the simulation of reentry flow conditions in a simple and cost-efficient way. For a better understanding of the processes occurring in a shock tunnel as well as for an optimal comparability of experimental data gained in shock tunnels to numerical simulations, it is highly desirable to have the best possible characterization of the generated test gas flows. This paper describes the final step of the development of a laser-induced grating spectroscopy (LIGS) system capable of measuring the temperature in the nozzle reservoir of a free-piston shock tunnel during tests: the successful adaptation of the measurement system to the shock tunnel. Preliminary measurements were taken with a high-speed camera and a LED lamp in order to investigate the optical transmissibility of the measurement volume during tests. The results helped to successfully measure LIGS signals in shock tube mode and shock tunnel mode in dry air seeded with NO. For the shock tube mode, six successful measurements for a shock Mach number of about 2.35 were taken in total, two of them behind the incoming shock ($p \approx 1$ MPa, $T \approx 600$ K) and four after the passing of the reflected shock ($p \approx 4$ MPa, $T \approx 1000$ K). For five of the six measurements, the derived temperatures were within a deviation range of 6% to a reference value calculated from measured shock speed. The uncertainty estimated was less than or equal to 3.5% for all six measurements. Two LIGS signals from measurements behind the reflected shock in shock tunnel mode were analyzed in detail. One of the signals allowed an unambiguous derivation of the temperature under the conditions of a shock with Mach 2.7 ($p \approx 5$ MPa, $T \approx 1200$ K, deviation 0.5%, uncertainty 4.9%).

Keywords Free-piston shock tunnel · LIGS · Laser-induced grating spectroscopy · LITA · High-temperature measurements

1 Introduction

The reentry process into the earth's atmosphere continues to remain one of the greatest challenges in manned spaceflight. At the same time, the flow conditions of this critical phase of the mission, in which speeds of 8–11 km/s need to be decelerated to approximately zero, are nearly impossible to be simulated in ground-based facilities due to the high energy of the flow. One way to reproduce at least parts of the reentry trajectory are free-piston shock tunnels like the High-Enthalpy Laboratory Munich (HELM) at the University of Federal Armed Forces Munich [1]. In test facilities like

this, transient shock compression is used to generate high-enthalpy and high-speed flows similar to reentry conditions for a few milliseconds. Another field of research, in which free-piston shock tunnels are used, is the investigation into air-breathing supersonic propulsion systems, also known as scramjets [2].

Since the results gained in shock tunnels are often used for validation of numerical simulations, it is necessary to have a detailed knowledge of the generated flows and therefore the test gas properties in the nozzle reservoir. Unlike for the pressure, which can be measured by standard-type piezoelectric sensors, the measurement of the temperature is more challenging. Conventional probes like thermocouples are too restricted by thermal, mechanical, and temporal limitations for this measurement task. Additionally, they would either influence the supersonic flow or only measure the wall temperatures of the shock tube. In order to overcome this restriction, HELM is the first piston-driven shock tunnel which was designed with an optical access at its noz-

Communicated by S. O'Byrne.

✉ T. Sander
tobias.sander@unibw.de

¹ Institute for Thermodynamics, University of Federal Armed Forces Munich, Werner-Heisenberg-Weg 39, 85577 Neubiberg, Germany

sure level is reached, the diaphragm bursts and the desired shock wave is generated in the shock tube.

Similar to the processes in a conventional shock tube, a contact surface between driver gas and test gas forms and runs behind the shock. In contrast to the conventional shock tube, the expansion is separated in two transient parts and one stationary part. This is caused by the cross-section reduction between driver and shock tubes. This reduction enables the piston, which is still in forward movement during the burst of the diaphragm, to sustain the pressure level in the driver tube, even when the first driver gas is expanding into the shock tube. This pressure “cushion” is also needed as an aerodynamic brake to avoid the impact of the piston in the area of diaphragm 1. As described above, the shock wave, which runs along the shock tube, is reflected at the Mylar diaphragm. This diaphragm gives in to the high pressure and high temperature behind the reflected shock instantaneously, allowing the generation of the high-energy high-speed flow by expansion of the standing test gas (state 5) through the Laval nozzle into the evacuated measurement chamber.

The measurement time in facilities like this is in the order of a few milliseconds and is restrained by the arrival of the contact surface at the Laval nozzle. To maximize the test time, the filling pressures of driver tube and shock tube have to be adapted to the used gases in such a manner that the contact surface is decelerated to zero by hitting the reflected shock. This so-called tailored state ensures a constant pressure level in the nozzle reservoir.

On the shock tunnel facility HELM, four piezoelectric pressure sensors of type PCB M111A22 are installed in total along the driver tube and shock tube to monitor the test sequence. The flush alignment of the sensors with the inner surface of the shock tube guarantees non-intrusive measurement of pressure. One sensor is installed at the end of the driver tube to observe the burst pressure of the first diaphragm and the above-mentioned development of the pressure “cushion.” Two sensors are positioned in a defined distance to each other along the shock tube to determine the time difference with which the shock passes these sensors. By dividing the derived shock speed by the speed of sound of the quiescent test gas, the Mach number of the shock can be calculated. Since the test gas properties p_1 and T_1 before the test are known, the shock relations for calorically perfect gas can be used to calculate reference values p_{ref} and T_{ref} from the measured Mach number M .

However, the pressure at the nozzle reservoir p_{meas} is also measured by the last pressure sensor. The pressure sensor is situated in the same vertical plane of the shock tube as the optical window. Due to deviations between measured pressures (p_{meas}) and calculated pressures (p_{ref}), a second comparative temperature T_p was determined. This was done by deriving a comparative Mach number M_p from the pressure ratio p_{meas}/p_1 . For this purpose, the shock relation given

in (1) was solved iteratively for M_p . γ herein is the isentropic exponent.

$$\frac{p_{\text{meas}}}{p_1} = \frac{2\gamma M_p^2 - (\gamma - 1) - 2(\gamma - 1) + M_p^2(3\gamma - 1)}{\gamma + 1} \frac{1}{2 + M_p^2(\gamma - 1)}. \quad (1)$$

The determined Mach number was used with the similar shock relation for the temperature behind a reflected shock to calculate the temperature T_p based on the measured pressure.

3 Laser-induced grating spectroscopy

As described in Sect. 1, the measurement task in the nozzle reservoir is very demanding in terms of measurement time, size of optical access, and levels of pressure and temperature. A detailed summary of the techniques taken into account and of the decision-making process in favor of laser-induced grating spectroscopy (LIGS) can be found in [3]. Nevertheless, a short overview on the considered measurement techniques and their main restrictions shall be given:

The application of LIF as a two-dimensional optical technique is strongly restricted due to the small dimension of the optical access. Furthermore, quenching processes in the high-pressure environment and broadband chemiluminescence from the heated gas would complicate the analysis of the LIF signal. The quantitative interpretation of the data gained from emission spectroscopy would require significant effort, as a detailed study of the chemical processes leading to the emission would be necessary.

Coherent anti-Stokes Raman spectroscopy (CARS), as well as laser-induced grating spectroscopy (LIGS), has the advantage of a coherent signal, meaning that a small optical access is sufficient. In contrast to absorption spectroscopy techniques like tunable diode laser absorption spectroscopy (TDLAS), both techniques offer a high spatial resolution in the measurement volume. Furthermore, the temperature measurement by TDLAS usually requires a measurement signal with a clear line shape of the absorption feature. In a high-pressure environment like the nozzle reservoir of a free-piston shock tunnel, pressure broadening would most likely impair the signal quality. Since a new measurement system had to be developed at the institute, one aspect favoring LIGS over CARS also was the very simple signal analysis of LIGS, which basically is a determination of frequency in the signal. The signal analysis of CARS in comparison is rather complicated.

Besides the coherence of the LIGS signal and the simple data analysis, the main advantages are that the signal quality of LIGS increases with increasing pressure and that potential absorbers for the generation of a thermal grating occur during shock compression at high temperatures. LIGS has already been successfully used in several shock-related [9,10] and

shock-tube-related [4,11] investigations in recent years. The highest levels of pressure and temperature, which have been reported to be investigated with LIGS in gaseous media and flames so far, are 14 MPa [12] and around 2300 K [13,14], respectively. In hydrothermal solutions, speed of sound measurements via LIGS was performed at pressures up to 70 MPa [15]. These investigations further encouraged the confidence in the feasibility of successful LIGS temperature measurements in the nozzle reservoir of the shock tunnel.

In this work, laser-induced grating spectroscopy is used as collective term for laser-induced thermal grating spectroscopy (LITGS) and laser-induced electrostrictive grating spectroscopy (LIEGS). Both techniques are based on different types of density gratings, which are described in detail below. In the literature, sometimes the term laser-induced transient grating spectroscopy (also LITGS) is used as collective term for LITGS and LIEGS (e.g., in [16]). However, this term is not used here in order to avoid the ambiguity of the shortening LITGS.

Due to the optoacoustic effect of the transient gratings, LIGS is also often denoted laser-induced thermal acoustics (LITA). If the measurement uses a thermal grating (based on absorption of the pump laser light), it is described as resonant LITA, and if a wavelength-independent electrostrictive grating is used, the description is non-resonant LITA. In addition, the kind of detection can be distinguished for LITA as well: During a homodyne detection only the measurement signal transient in time is recorded, which results from the refraction of the probe beam on the induced grating. This signal allows the measurement of sound velocity, pressure, thermal diffusivity, and further gas properties [17]. Under certain conditions, concentrations and the temperature can also be determined [18,19]. For a heterodyne detection, a part of the probe beam is detected as reference beam supplementary to the measurement signal. By superimposing the reference beam with the signal, the fluid velocity in the test gas can be measured by using the Doppler effect. However, by using an intended misalignment of the optical setup this can also be realized for homodyne detection [20]. For this work only the homodyne detection was used.

3.1 Measuring principle and signal processing

The physical background of the formation of laser-induced gratings and their reading is described in detail in [17–19,21]. For the sake of completeness, a sketch of the arrangement of the laser beams in the measurement volume (Fig. 2) and the essential equations shall be shown here.

The laser-induced grating is formed at the intersection of two coherent pulsed pump beams (wave vectors \mathbf{k}_1 and \mathbf{k}_2 , wavelength λ_{pump}) with a crossing angle Θ . The grating induced by the interference of the beams has a vector \mathbf{q} , and

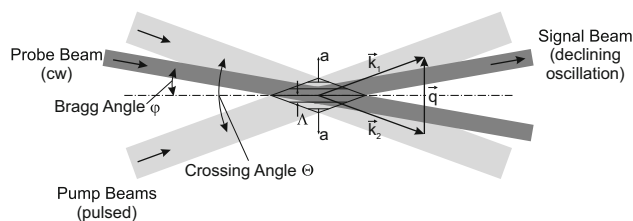


Fig. 2 Schematic of the crossing laser beams [3]

its constant Λ depends on the wavelength of the pump beams and the crossing angle:

$$\Lambda = \frac{\lambda_{\text{pump}}}{2 \sin(\Theta/2)}. \quad (2)$$

Generally two laser-induced grating types may develop, with usually one of them being dominant: a non-resonant electrostrictive grating (LIEGS) and a resonant thermal grating (LITGS). The predominance depends on the test gas composition and the settings of the optical setup [2]. As a result, a density interference pattern develops, based on the polarization of molecules (LIEGS) and based on the absorption of laser light (LITGS). The resulting acoustic waves move in opposite directions, parallel to the grating vector \mathbf{q} , causing constructive and destructive modulation of the scattering efficiency in the medium. This modulation shows up as a cyclical variation in the intensity of a scattered continuous wave probe beam (wavelength λ_{probe}), which intersects the measurement volume at Bragg angle φ . The Bragg angle condition can be written as:

$$2 \sin \varphi = \frac{\lambda_{\text{probe}}}{\Lambda}. \quad (3)$$

The corresponding oscillation frequency f_M of the intensity of this generated signal beam can be expressed by (4), where a is the sound velocity of the test gas and $c = 2$ for an electrostrictive and $c = 1$ for a thermal grating:

$$f_M = c \frac{a}{\Lambda}. \quad (4)$$

Because of heat conduction and diffusion, the density grating induced in the gas and therefore also the intensity of light scattered from the grating decays with time. By analyzing the signal beam with a discrete fast Fourier transform (FFT), the oscillation frequency f_M of the induced grating can be measured. If the grating constant Λ and the type of the grating are known, the sound velocity in the test gas can be calculated easily by solving (4).

Because it is very difficult to measure the exact crossing angle Θ in the experimental setup to obtain the grating constant, a reference measurement (average of 1000 signals) is

done at room temperature and elevated pressure after calibration of the setup and before every set of experiments. The sound velocity for the reference point is determined by interpolation of real air data provided in [22] over known pressure and temperature. Using the measured oscillation frequency and the sound velocity of the reference point in (4), the grating constant of the setup can be calculated.

As mentioned earlier, the knowledge of the grating constant then allows derivation of the sound velocity of the test gas in the experiment from the oscillation frequency measured. For the shock tunnel tests, the frequency with the strongest peak in the range of 38–75 MHz (corresponding to temperatures between 450 and 1800 K) was identified in the result of the FFT analysis. The corresponding measured temperature T_{LITGS} of the test gas was then gained by a backward interpolation of the data in [22], taking into account the pressure p_{meas} , measured in the nozzle reservoir during LITGS signal acquisition, and the sound velocity calculated by solving (4) with the measured frequency.

A typical measured LITGS signal obtained during the tests in shock tube mode is shown in Fig. 3. The signal was processed by using the software MATLAB [23]. The solid black line is the part of the signal that was used for the FFT. Due to the strong noise and background structure, only the parts of the signals with the strongest oscillations could be used. For these first shock tunnel tests presented here, the useful part of the signal was identified and defined manually. The unused parts of the signals are faded out in gray color. Additionally, a median line, which is shown as dotted curve, was subtracted from the signal as part of the data processing. It was determined by using the smoothing function of the curve fitting toolbox of MATLAB with a moving average filter of large span. The result of the FFT is shown in right lower corner. The peak was identified using the “max” function of MATLAB.

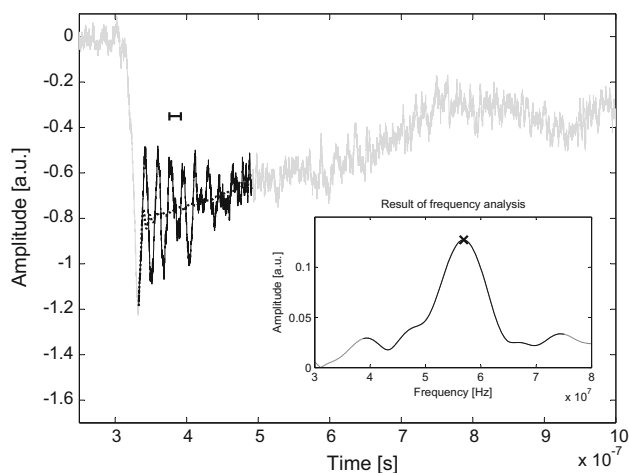


Fig. 3 Typical LITGS signal obtained in shock tube mode ($M = 2.33$, $p_{\text{meas}} = 4.08$ MPa, $T_{\text{LITGS}} = 982$ K) [7]

Furthermore, the two frequencies for 98% of the maximum amplitude were identified in order to verify the symmetry of the peak. For all investigated signals, the found asymmetries led to variations smaller than 3 K in the derived temperature and were therefore neglected. The oscillation period of the determined strongest frequency is shown as a small black horizontal line in the upper left corner of the figure.

3.2 Optical setup

As mentioned before, two major challenges had to be overcome with the optical setup: the more restricted optical access (in comparison with previous measurements on the pressure chamber and the conventional shock tube) and a significant lateral movement of the shock tube in the range of several centimeters.

The optical access at the HELM nozzle reservoir consists of three tubes, each 250 mm in length and 25 mm in diameter, in a 0° – 90° – 180° -constellation. This arrangement allows the detection of laser light that passes the reservoir in linear direction as well as the detection of scattered light in rectangular orientation of the passing laser beam. Even if an internal design for the optical access window was evaluated as the best solution in terms of aerodynamic perturbations and losses, an external design was chosen due to the benefits in clear span and the easier and thus cheaper manufacturability. The realized design is shown in Fig. 4.

The sapphire window has a thickness of 15 mm, a total diameter of 38 mm, and a clear span of 25 mm. For vacuum tightness, an O-ring is fixed between the window and the shock tube. In terms of high pressure, an NBR mat tightens the window, while a copper sealing tightens the window holder. An additional O-ring keeps the window in place and

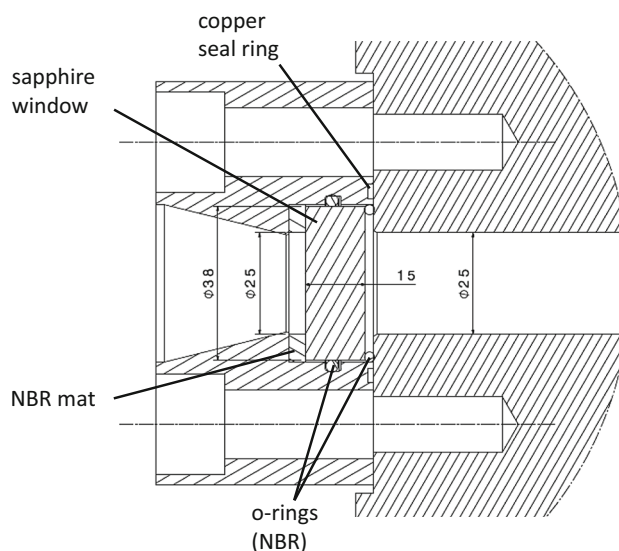


Fig. 4 Design of the external shock tube window [7]

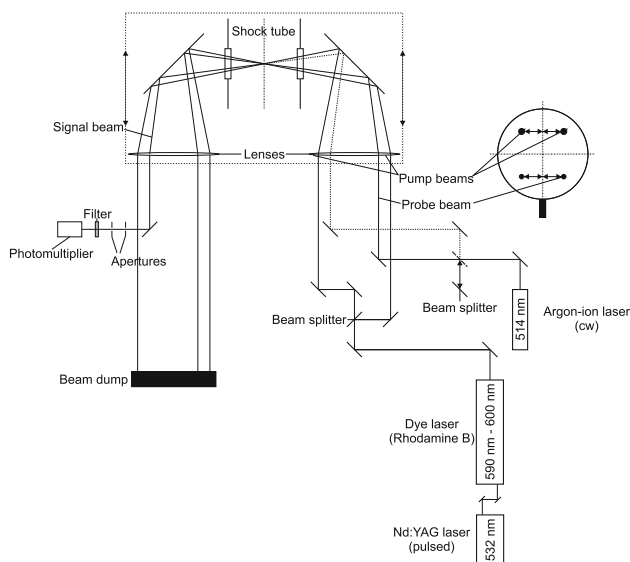


Fig. 5 Scheme of the LITGS setup on the free-piston shock tunnel HELM [25]

ensures that the window is not in contact with any steel parts [24]. Otherwise, shock waves traveling through the steel of the shock tube during the test could destroy the window.

A top view on the optical setup of the LIGS system at the shock tunnel is shown in Fig. 5. Similar to the setup described in [4], the pump beams are generated by sending the output of a dye laser, pumped by a Nd:YAG-laser, on a beam splitter. The two pump beams, which have a wavelength of 593 nm (λ_{pump} , cf. Sect. 3.1), are then aligned parallel to each other and the shock tube. Furthermore, they are running in a distance of 13 mm to the vertical middle axis of the converging lens and symmetrically to this axis. This ensures that the beams intersect in the right angle. The probe beam is generated by an argon-ion laser at 514.5 nm (λ_{probe} , cf. Sect. 3.1). This continuous wave beam is also aligned in parallel with the two pump beams and the shock tube, however, with a vertical offset of about 12 mm to the pump beams. The distance from the vertical axis of the lens is about 11.3 mm for the probe beam. The measurement volume resulting from this configuration is estimated to a length of 9.6 mm and a diameter of 250 μm . The focal point of the converging lens, and hence the measurement volume, is positioned in the middle of the shock tube diameter of 95 mm to measure the temperature right in the core of the flow profile.

By shifting an additional beam splitter in the beam path of the probe beam, the beam path of the signal beam can be simulated for calibration purposes and the alignment of the detection optics. These consist of beam dumps for the pump beams and the probe beam and of a photomultiplier system with several apertures and an optical band-pass filter for the signal beam. Unlike the system described in [3], the converging lens here is fixed to the shock tunnel to account

for the recoil movement of the facility. Due to the parallel alignment of the beams, the lateral position of the lens during impact of the beams is meaningless. Together with the 500-mm lens, a mirror is attached to the window holder to direct the beams into the nozzle reservoir. An identical setup is chosen for the detection side: The beams are parallelized again after passing the measurement volume to allow the detection with a fixed setup despite facility movement. The detection system consists of a TSI photomultiplier of type 9162 and a LeCroy oscilloscope of type WaveRunner 104XI-A with bandwidths of 200 MHz and 1 GHz, respectively.

4 Results

In total, 63 shock tunnel tests were conducted to obtain the results presented in this paper. During the first 39 measurements, the HELM facility was operated in shock tube mode. By using a solid end instead of a nozzle, the chance of successful LIGS measurements was expected to be increased due to less test gas movement during the measurement. The remaining 24 tests were performed with nozzle, hence in shock tunnel mode. Eight out of these 63 tests failed due to problems with diaphragms (seven) or the triggering of the optical setup (one).

4.1 Preliminary measurements

During the first unsuccessful measurement attempts in shock tube mode, observations on the optical transmittance of the continuous probe beam showed a deterioration for several seconds after the first detection of the shock. In order to gain a better understanding of the phenomena, three tests (two in shock tube mode/one in shock tunnel mode) were performed to measure the optical transmissibility of the measurement volume throughout the test. Therefore, a LED lamp was placed in front of the lens on the laser side of the setup and a Redlake HG-100K high-speed camera was placed on the photomultiplier side.

The result of the second test in shock tube mode is shown in Fig. 6. The condition for the test was a shock Mach number of 2.46 at a shock tube filling pressure of 0.25 MPa (dry air). The frame rate of the camera was set to 10,000 fps at a resolution of 256×256 pixels. In total, 505 pictures were taken with an exposure time of 5 μs each. The curve shows the pressure measured by the pressure transducer positioned at the nozzle reservoir, i.e., the measurement volume, during the test. The filling pressure of 0.25 MPa was raised to a level of about 1.8–1.9 MPa by the incoming shock. After the passing of reflected shock, the pressure overshoot to about 7.5 MPa before it stabilized at a level of about 5.5 MPa. On the top end of the chart, the moments are marked by a cross when an image was recorded. Right above each cross

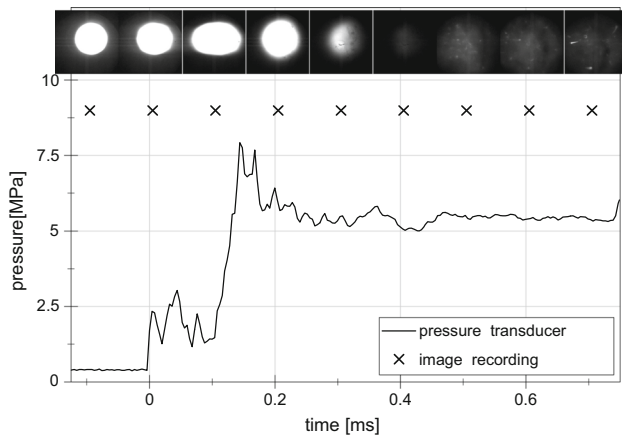


Fig. 6 Optical transmissibility in shock tube mode (10,000 fps, 256×256 pixels) [7]

the corresponding image is shown. The first image on the left shows the situation before the incoming shock passed the optical access at the nozzle reservoir. The circular spot represents the long tubes of the optical access illuminated by the LED lamp. Images 2 and 3 show a distortion of the circle caused by the passing of the incoming and later the reflected shock and potentially also due to the movement of the shock tube. It can be seen on the fourth picture that right after the pressure overshoot the light passed the measurement volume mostly undisturbed. Shortly afterward, the pictures darken rapidly, showing that nearly no light was able to pass through the optical access anymore and thus confirming the previous observations. Except of a few single sparks and a very small glimmer on the first pictures (7–9), the measurement volume remains obscured for the rest of the recording. Right after the test, raised dust could be observed in the shock tube, obviously causing the shading of the LED light. The other transmissibility test in shock tube mode was recorded with 5000 fps and a resolution of 512×512 pixels and showed a very similar result.

The third and last measurement of optical transmissibility was performed in shock tunnel mode. At a Mach number of 2.42, dry air seeded with NO/N₂ mixture (1650 ppm) to a NO concentration of 220 ppm was used as the test gas. The filling pressure of the shock tube was 0.15 MPa. The settings of the high-speed camera were the same as for the second measurement in shock tube mode apart from the number of pictures taken (5005 pictures). The result of this measurement is shown in Fig. 7. The first picture again shows the undisturbed status before the passing of the shocks. On the second to fifth picture, it is clear that the circular spot is imaged with light distortions but mostly undisturbed after the passing of the incoming and the reflected shocks. There was no darkening of the pictures taken afterward. However, from the sixth image on it can be observed that the boundaries of

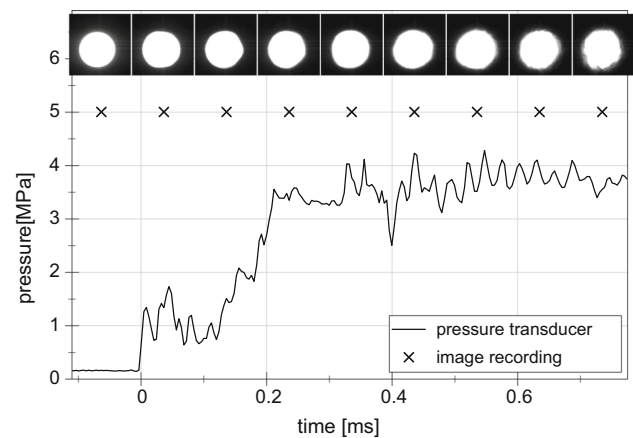


Fig. 7 Optical transmissibility in shock tunnel mode (10,000 fps, 256×256 pixels) [7]

the bright circle start to become blurred. This situation lasted to the end of the recording.

Based on these preliminary measurements, the temporal delay between trigger pulse and laser pulse was minimized to 205 μ s for all LITGS measurements in shock tube mode, which were triggered by the pressure sensor positioned directly at the optical access. This ensured that the laser beams and the signal beams passed the measurement volume before obscuration set in. Additionally, a laser energy measurement sensor was used for the collection of the pump beams instead of a beam dump (cf. Fig. 5). By measuring the energy of the passing laser pulse quantitatively, this setup allowed immediate determination of the level of darkening in the nozzle reservoir. Another measure to improve the chances of successful measurements was a thorough cleaning of the whole shock tunnel facility between each test to avoid raising of particles of former tests during the shock passage.

Since all the test gas (including potential particles carried in it) is blown through the nozzle during each test in shock tunnel mode, no measures in terms of cleaning were necessary here. However, due to the blurred boundaries seen during the transmissibility tests in shock tunnel mode, the optical setup of the LIGS systems was optimized. Therefore, the distances of the impact points of the lasers on the first converging lens to the middle of the lens were minimized as far as possible. This measure assured that the laser beams were not diffracted in the blurred boundaries of the optical passage area.

In general, the measurements showed that an optical transmissibility of the measurement volume shortly after the passage of the reflected shock was given. Therefore, it was assumed most likely feasible to perform successful optical temperature measurements in the nozzle reservoir during the generation of the high-speed flow in a free-piston shock tunnel.

4.2 LITGS measurements in shock tube mode

The optimization of the measurement setup driven by the results of the preliminary measurements allowed successful temperature measurements on the shock tunnel in shock tube mode. To raise the chances of success, moderate test conditions were chosen. The used steel diaphragms had a burst pressure of about 5 MPa leading to Mach numbers of 2.3–2.4 in a shock tube filled to a pressure of 0.15 MPa. The pressure and temperature in the nozzle reservoir resulting from these starting conditions were around 1 MPa and 600 K, respectively, for the incoming shock and about 4 MPa and 1000 K, respectively, for the reflected shock.

The driver gas was dry air with a filling pressure of 0.1 MPa compressed by a piston made of aluminum with a weight of 57.6 kg. Since thermal gratings are assumed to suit the high-temperature conditions better than the electrostrictive gratings, the test gas was seeded with nitrogen monoxide (NO). This was done by filling the formerly evacuated driven tube with a NO/N₂ mixture of 1650 ppm to a pressure of 0.01 MPa. Afterward, the driven section was pressurized up to the nominal pressure of 0.15 MPa with dry air additionally. Thus, the final test gas had an initial seeding of 110 ppm nitrogen monoxide.

In total, six successful measurements could be taken in shock tube mode. Measurements M1 to M3 were triggered by a pressure sensor 3.65 m upstream of the measurement position, thus allowing measurements after passing of the incoming shock. However, due to small variations in the shock speed from test to test, the relative time of measurement to the shock passing varied. Therefore, measurement M3 coincided with the passing of the reflected shock. For the measurements M4 to M6, pressure rise due to the incoming shock at the pressure transducer positioned directly at the nozzle reservoir was used for triggering to ensure that the time of measurement will be after the passing of the reflected shock.

The sound velocities calculated from the measured frequencies and the temperatures derived from them via real air data interpolation are summarized in Table 1. The first column gives the measured Mach numbers of the test. It

can be seen that there is a variation from 2.33 to 2.41. By using these Mach numbers and the filling pressure of the shock tube before the test, reference temperatures and reference pressures can be calculated from the common shock relations for ideal gas. These pressures p_{ref} and temperatures T_{ref} are listed in columns 2 and 4, respectively. The third column shows the pressure p_{meas} measured in the nozzle reservoir during the acquisition of the LITGS signal. As mentioned above the first two signals were obtained behind the incoming shock, resulting in lower pressures and temperatures compared to the rest of the measurements.

Columns 6 and 7 list the results of the LITGS measurement in form of the measured sound velocity a_{LITGS} and backward-interpolated temperature T_{LITGS} , respectively. In column 8, the signal-to-noise ratio of the FFT analysis (SNR_{FFT}) in the investigated frequency range is given as an indication of the signal's quality. It is calculated from the ratio of highest to the second highest peak in the frequency analysis. The alternative reference temperature T_p calculated from the pressure ratio of p_{meas} and the shock tube filling pressure fills the fifth column. The deviations $T_{\text{LITGS}} - T_{\text{ref}}$ and $T_{\text{LITGS}} - T_p$ given in percentage (referred to the reference temperature) are presented in columns 9 and 10, respectively.

In Fig. 8, all the measurement results and schematic temperature traces for T_{ref} are visualized for the different Mach numbers.

The curve shape of the temperature traces reflects the main slope of the measured pressure traces: After a steep rise due to the incoming shock ($t = 0$ ms) and a fairly stable plateau, the pressure jump is a bit less steep for the reflected shock ($t = 0.1$ – 0.15 ms). This slope in the transition from initial to reflected shock condition is caused by unclean shock reflection (cf. Fig. 7). As described in Sect. 3.2, the three tubes of the optical access lead to aerodynamic perturbations and losses in the nozzle reservoir. The gray tones of the LIGS results were adapted to the Mach number measured during each test. The meaning of the error bars is described in the next paragraph.

There were significant variations in the quality of the measurement signals. The LITGS signals in the incoming shock had a comparatively low level of noise and background

Table 1 LITGS results obtained in shock tube mode ($M \approx 2.35$) [7]

	M (–)	p_{ref} (MPa)	p_{meas} (MPa)	T_{ref} (K)	T_p (K)	T_{LITGS} (K)	a_{LITGS} (m/s)	SNR_{FFT} (–)	ΔT_{ref} (%)	ΔT_p (%)
M1	2.38	0.97	1.05	593.7	622.1	589	485	1.79	– 0.9	– 5.4
M2	2.41	0.99	0.97	601.4	593.9	571	478	2.79	– 5.1	– 3.9
M3	2.33	3.69	4.02	925.4	971.6	984	623	1.26	6.4	1.3
M4	2.33	3.69	4.08	925.4	978.4	982	623	3.78	6.1	0.3
M5	2.36	3.82	4.25	941.0	999.4	1124	663	2.58	19.5	12.5
M6	2.33	3.69	3.98	925.4	966.2	870	589	5.14	– 6.0	– 10.0

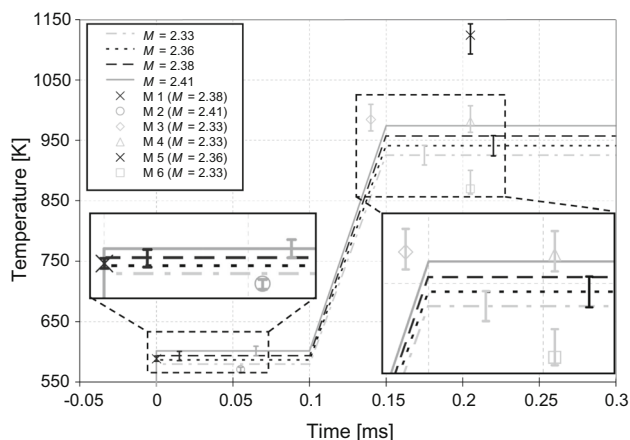


Fig. 8 Schematic reference temperature traces and measured LIGS temperatures in shock tube mode [7]

structure, most likely due to moderate pressures, moderate temperatures, and lower vibrations in the facility during the beginning of the test. The signal-to-noise ratio of the LITGS raw signal (SNR) was determined by dividing the height of the amplitude of the oscillation by the height of the noise in the signal. For the measurement M1, the SNR went from 7.2 at the beginning of the signal to 1.7 after the eighth oscillation. For the measurement M2, these values were only 2.1 and 1.2, respectively, because a surprisingly strong LIGS signal led to a saturation of the photomultiplier detection system. Nevertheless, plausible temperature information could be derived from the signal. For the FFT analysis, unambiguous SNR_{FFTs} of 1.79 and 2.79 were derived for M1 and M2, respectively.

Most of the measurements in the reflected shock also showed good signal quality, even if noise and background structure were increased. Only measurement M3, which was taken during the passing of the reflected shock, was of marginal quality. The SNRs for the measurements M3 to M6 were 1.8, 5.1, 3.8, and 3.2 at the beginning of the signal, respectively. Due to the higher temperature behind the reflected shock than for the incoming shock, the signals had fewer oscillations. The SNRs at the end of the signals were therefore determined after the fifth oscillation to 2.3, 2.0, and 1.8 for M4 to M6, respectively. For M3, no clear signal could be identified any further at this stage. SNR_{FFTs} of 1.26, 3.78, 2.58, and 5.14 were obtained for the FFT analysis of the four measurements M3 to M6.

It can be seen in Fig. 8 that the successful measurements well represent the evolution of temperature during the passing of the shocks. For the incoming shock, the deviation between the measurements and the reference temperatures derived from the Mach numbers is at 5.1% maximum. The deviations for the reflected shock are mainly in the area of 6%; only measurement M5 represents an outlier with around 20%.

Since for the reflected shock measurements the measured pressures lie significantly above the calculated pressures, the alternative reference value T_p was calculated as described before. Based on this value, the deviations decrease to 12.5% maximum for the reflected shock and slightly increase to 5.4% for the incoming shock. In total, four of six measurements show better results for the alternative reference value. Not shown here is the comparison of LIGS temperature with a reference value calculated from measured pressure under the assumption of isentropic change as applied in [11,26]. The values determined for isentropic change were roughly in the middle between T_{ref} and T_p , and the overall deviation for the six measurements was not smaller than the deviation to T_p .

It has to be considered that the reference values calculated with one-dimensional shock equations for ideal gas do not provide exact values. That is not only because of three-dimensional aerodynamic effects, viscosity effects, or non-ideal gas effects, but also due to unavoidable measurement errors of the input values. The Gaussian law of error propagation [27] can be used to estimate the influence of different measurement errors on the reference value. The results are shown as error bars in Fig. 8 near the correlated measurement. For the incoming shock, an uncertainty of ± 7.7 K (shown at 0.015 ms) and of ± 7.9 K (shown at 0.065 ms) are estimated for Mach numbers of 2.38 and 2.41, respectively. The impact was increased for the reflected shock: the calculation resulted in an uncertainty of ± 16.3 K (shown at 0.175 ms) and ± 16.8 K (shown at 0.22 ms) for the Mach numbers of 2.33 and 2.36, respectively.

As clearly obvious in Fig. 8, there is still some distance between the LIGS measurements and the error bars of the reference values. This is caused by the uncertainty of the LIGS measurement and its processing routine. One essential aspect here is that for the determination of the sound velocities and temperatures real air data [22] were used. However, the used test gas was air seeded with a significant amount of NO diluted in N₂ (1650 ppm). The effect on the determined sound velocity $\Delta a_{seeding}$ and thus temperature $\Delta T_{seeding}$ was estimated by considering the changed molecular mass of the test gas. The values were recalculated via the ideal gas equation ($a^2 = \gamma RT$), and the results are summarized in Table 2.

It can be assumed that the behavior of the isentropic exponent γ of the test gas does not change due to the seeding, as the seeding components NO and N₂ are diatomic molecules like the main components of dry air, N₂ and O₂. If in the mentioned ideal gas calculations for estimation of $\Delta T_{seeding}$, the temperature-dependent and pressure-dependent isentropic exponent for real gas air from [22] is used instead of a constant value of 1.4; uncertainties ΔT in the same order of magnitude can be determined (see Table 2), however with opposite direction. The thusly estimated uncertainties are also shown as error bars for each measurement in Fig. 8.

Table 2 Uncertainties of LITGS measurements in shock tube mode [7]

	$\Delta T_{\text{seeding}}$ (K)	$\Delta a_{\text{seeding}}$ (m/s)	ΔT (K)
M1	- 4.4	- 1.1	4.5
M2	- 4.9	- 0.7	3.8
M3	- 18.9	- 1.5	25.2
M4	- 18.4	- 1.5	25.7
M5	- 31.1	- 1.5	18.8
M6	- 8.7	- 1.4	30.7

In terms of the processing routine, two more potential sources of uncertainty were identified: In order to estimate the effect of variations in oscillation frequency on obtained temperatures, the frequencies determined in the LITGS measurements M1 and M4 as an example were varied by ± 1 MHz. The resulting variation in LITGS temperature was around ± 30 K for the measurements after the incoming shock and around ± 40 K for the measurements after the reflected shock. If these variations are scaled with an uncertainty relevant for this investigation, e.g., the resolution of the frequency in the FFT analysis of 76 kHz, an uncertainty of derived temperature of approximately 3 K can be calculated. Furthermore, as described in Sect. 3.1 only the strong parts of the LITGS raw signal were used for the FFT analysis, and the determination of these signal parts was performed manually. By as an example varying the position of the first and second cut by ± 100 data points for the signal of M4, a maximum temperature variation of 11.3 K was found. In respect of the estimated uncertainties due to seeding, which are given in Table 2, these uncertainties of 3 and 11.3 K introduced by the processing routine are negligible.

Due to the low number of tests, no mean value or standard deviation was determined for the set of measurements. In consideration of the high effort that was necessary to yield the presented measurements (37 shock tunnel tests for six measurements), it was not possible to provide a meaningful statistical analysis in the frame of this work.

4.3 LITGS measurements in shock tunnel mode

After successful measurements in shock tube mode, the LITGS system was also used for HELM tests in shock tunnel mode. In order to avoid confusion, the measurements in shock tunnel mode are denoted with “V” (instead of “M”). In spite of the results of the preliminary experiments, which promised higher chances for the shock tunnel mode, only one unambiguous LITGS measurement was obtained from 20 successful HELM tests. This measurement V1 had a diaphragm burst pressure of around 8 MPa leading to a shock Mach number of 2.71 and therefore to pressures and temperatures behind the reflected shock of 5 MPa and 1200 K,

respectively. Another temperature was derived from an additional measurement signal V2, however with a poor SNR. For this test, the diaphragm burst pressure of 15 MPa generated a pressure of 7 MPa and a temperature of 1400 K behind the reflected shock.

Just like the tests in shock tube mode, all tests were performed with the aluminum piston of 57.6 kg. To increase the chances of successful measurements, the test gas (dry air) was seeded again with a NO/N₂ gas mixture (1650 ppm NO). The filling pressure of the shock tube was also 0.15 MPa, however, this time with a seeding of 330 ppm NO. The measurements were taken approximately 250 μ s after the passing of the incoming shock, where the pressure level was stable after a small overshoot caused by the shock reflection. The pressure transducer positioned at the optical access was used as the trigger. The signals were processed as described before, and

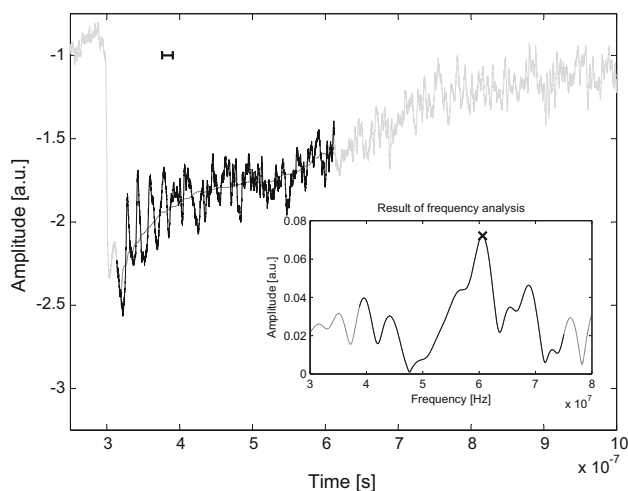
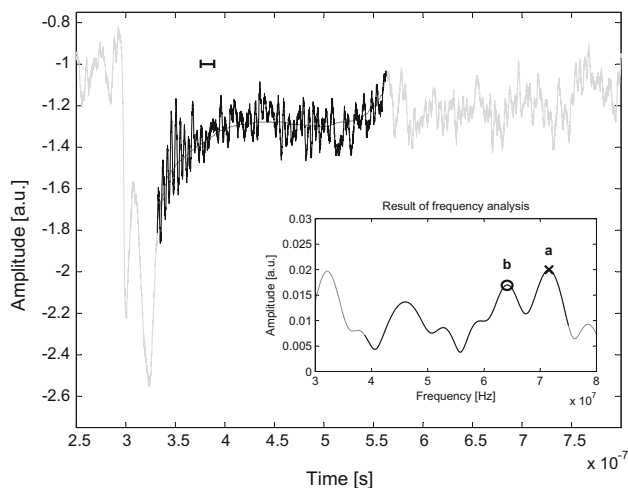
**Fig. 9** LITGS signal and result of FFT analysis for measurement V1 obtained in shock tunnel mode [7]**Fig. 10** LITGS signal and result of FFT analysis for measurement V2 obtained in shock tunnel mode [7]

Table 3 LITGS results obtained in shock tunnel mode [7]

	M (–)	p_{ref} (MPa)	p_{meas} (MPa)	T_{ref} (K)	T_p (K)	T_{LITGS} (K)	a_{LITGS} (m/s)	SNR_{FFT} (–)	ΔT_{ref} (%)	ΔT_p (%)
V1	2.71	5.77	4.76	1199.4	1061.9	1194	683	1.56	– 0.4	12.5
V2a	3.01	7.83	6.73	1429.4	1289.6	1684	806	1.17	17.8	30.6
V2b	3.01	7.83	6.73	1429.4	1289.6	1330	722	0.85	– 7.0	3.1

the results are shown in Figs. 9 and 10. Figure 9 shows the successful, unambiguous LITGS measurement V1. Despite strong noise, the typical LIGS signal shape with its oscillations can be recognized. The result of the FFT analysis is shown in the right lower corner of the diagram, and the small bar in the left upper corner gives the period of the determined oscillation frequency. Figure 10 is based on the second measurement V2: the typical oscillations cannot be identified, because a strong noise in the frequency range of 200–250 MHz is superimposed on the signal. The frequency analysis shows that the strongest frequency (a) is only little stronger than a second frequency (b). The marked period of the oscillation cannot be found in the signal by eye.

The summary of the analysis results is given in Table 3. For the test V2, a temperature was derived for the frequency with the strongest amplitude (V2a) as well as for the frequency of the second strongest peak (V2b). The reference values T_{ref} and reference values calculated by the measured pressure T_p were determined the same way as for the measurements in shock tube mode.

The qualities of the two measured signals differ strongly: While for V1 a SNR of about 3 at the beginning and about 2 after some oscillations leads to a SNR_{FFT} of 1.56 in the FFT analysis, no LIGS signal can be identified for V2 with the eye. This means the SNR of V2 is about 1. The side peak V2b in the frequency spectrum leads to a poor SNR_{FFT} of 1.17 for the FFT analysis as well.

It can be seen in Table 3 that for V1 the temperature measured with LITGS matches perfectly with the derived reference temperature T_{ref} . The deviation is only 0.4%. For V2a, however, the deviation is significantly greater. The LITGS temperature overshoots the expected reference temperature by 17.8%. This changes, if V2b is chosen for the determination of a LITGS temperature: The deviation decreases to about 7.0%. The comparison of the measured temperatures with the reference values T_p calculated by the measured pressure increases the deviations for V1 and V2a drastically to 12.5 and 30.6%, respectively. On the other hand, for V2b the deviation decreases further to 3.1%.

The reasons for the discrepancy between measurement and reference values were already described for the shock tube mode measurements. However, in the case of V2, certainly the poor signal quality and the resulting low SNR are the main reasons. Based on the knowledge that for the

Table 4 Uncertainties of LITGS measurements in shock tunnel mode [7]

	$\Delta T_{\text{seeding}}$ (K)	$\Delta a_{\text{seeding}}$ (m/s)	ΔT (K)
V1	– 58.0	– 4.5	5.7
V2a	– 101.4	– 4.3	0.3
V2b	– 59.5	– 3.8	22.1

given conditions a temperature between 1300 and 1400 K is expected, it can be assumed that the second strongest peak V2b in the FFT analysis is the actual signal. In conclusion, it can only be stated that the signal was too weak for an unambiguous and reliable temperature derivation.

The overall uncertainties for the reference temperatures T_{ref} due to error propagation were estimated to ± 25.8 and ± 34.9 K for V1 and V2, respectively. The uncertainties of the measured LITGS temperatures due to seeding and the variable isentropic exponent are shown in detail in Table 4. The overall length of the resulting LITGS error bars is in the same order of magnitude as the error bars of the reference temperatures. The variation in temperature due to the processing routine was as an example determined for V1 to circa 3 K for the resolution of the frequency in the FFT analysis and to 11.2 K for the variation of the signal bounds. Equally to the measurements in shock tube mode, these uncertainties are regarded negligible in comparison with the uncertainty introduced by the seeding.

From Tables 2 and 4, it can be seen that the error due to seeding is smaller in the sound velocity than in the temperature: While the error in temperature due to seeding adds up to 4.9, 6.0, and 4.5% for V1, V2a, and V2b, respectively, the error in the sound velocity only comes to 0.7% for V1 and 0.5% for V2a and V2b each. Similar results were obtained for the measurements M1 to M6 in shock tube mode (maximum error in temperature 3.5%, maximum error in sound velocity 0.24%). Therefore, for future applications, it seems reasonable to use the sound velocity to compare numerical simulations with LIGS measurement results in order to avoid unnecessarily high uncertainties.

4.4 Discussion

As mentioned in the previous sections, the overall success rate of LITGS measurements was quite low with eight suc-

successful measurements out of 63 experiments. In shock tube mode, this was to some extent caused by the obscuration due to raised dust, which is described in Sect. 4.1. However, after the adaptation of the system and during the measurements in shock tunnel mode, the success rate and signal quality were not satisfactory.

One reason for the poor success rate and signal strength of the LIGS signals during the performed shock tunnel tests might have been beam steering effects. Since the system was calibrated at shock tube filling pressure before each test, the system could have been slightly misaligned for the higher pressures after the reflected shock due to the change in refractive index of the test gas. For conditions M6 and V2, the shift of the focal point was estimated to 1.4 and 1.6 mm toward the rear wall of the shock tube, respectively. It seems likely that this shift led to a divergent signal beam, and thus, the signal beam on the photomultiplier lost strength due to the fixed apertures. This divergence was probably also observed when the LED lamp's spot on the CCD chip of the high-speed camera, shown in Fig. 7, slightly increased in diameter after the passing of the reflected shock. In future works, the calibration of the optical setup needs to be adapted to the shift of the focal point according to the expected pressure in the nozzle reservoir.

Another point, which does not only concern the LITGS success rate and signal quality, but also the performance of the shock tunnel and the determined reference temperature, is the disturbance of the shock reflection in the nozzle reservoir. This is caused by the additional volume of the tubes of the optical access. As described in Sect. 4.2, these perturbations lead to a less steep pressure jump from initial to reflected shock condition. Even if the main part of the deviation between LIGS measurements and reference temperatures T_{ref} and T_p is caused by the poor quality of the LIGS signals, it is clear that there is a significant uncertainty in the reference values introduced by non-ideal shock compression of the test gas. Furthermore, it cannot be excluded that aerodynamic turbulence phenomena in the tubes cause small movements of the optical access windows and thereby lower the chances of successful measurements. In order to minimize the effect of the optical access on the performance of the shock tunnel and the LITGS measurements, internal shock tube windows are currently under design, which will be flush-mounted to the inner shock tube wall. For this configuration, the measured pressures are expected to correlate much better with the predicted ones. This should make the calculation of a T_p unnecessary.

In order to increase the success rate of the laser measurements, a more detailed analysis of the shock tunnel movement during tests could be helpful. During this work, several videos of the tunnel were taken that show that there seems to be no relevant vertical movement of the facility in the time of LITGS measurement. However, the maximum frame rate of

the used camera was only 50 fps. Investigations with faster cameras might show vibrations or small vertical movements which deteriorate the LIGS signal. In this case, measures will have to be taken to account for it. This could be either a modification of the shock tunnel (e.g., installation of a damping system) or a reconfiguration of the optical setup from mirrors and windows to fiber optic coupling.

Some minor changes of the presented optical setup are also deemed appropriate to increase LITGS signal strength for future measurements: In a first step, the beam profile of the pump beam could be homogenized by using a spatial filter. Despite several readjustments of the dye laser, the beam profile did not show the desired quality. In a second step, a strip-shaped beam profile could be generated and used for the pump beams. With this modification, additional oscillations and a longer grating lifetime can be obtained in the LITGS signal [14], leading to a higher SNR_{FFT} in the FFT analysis. A last step of improvement could be a change in the used laser wavelengths: By switching the pump beam to a frequency-doubled Nd:YAG-laser at 532 nm, the effective absorption cross section of NO_2 can be approximately doubled [28,29]. A higher absorption rate would also lead to a stronger LITGS signal. However, due to the spectral vicinity of the 532 nm to the used 514.5 nm of the argon-ion laser, a different laser wavelength will be needed for the continuous probe beam, in order to allow a clear separation of signal beam and pump beam stray light.

Despite the described potential for improvement of success rate and signal quality, the current optical setup in the meanwhile was successfully used for a series of 10 shock tunnel tests under constant low-enthalpy conditions (1100 K, 6 MPa, 110 ppm NO). The results of this investigation are published in [30]. The precision (single-shot relative standard deviation) of FFT-analyzed LITGS signals here was determined to 3.88%. The accuracy in the form of mean temperature relative deviation was found to be -1.82% , while the intrinsic relative standard deviation of reference temperatures derived from incident shock Mach number was assessed to 2.86%. After the general proof of technical feasibility during this work, these measurements clearly show that at least for low-enthalpy conditions, accurate and reliable temperature information can be gained in the nozzle reservoir of a shock tunnel by use of the LIGS technique.

When it comes to higher enthalpy conditions, it is very difficult to predict at which level the limits of this technique might exist. One minor aspect is that the presented data processing routine is based on equilibrium air data for a temperature range till 2000 K and a pressure range till 2000 MPa [22]. While the pressure range is not critical, temperatures above 2000 K are typical for tests in the nozzle reservoir of a free-piston shock tunnel. An iterative approach using temperature-dependent approximations for the speed of sound in real gas air (which can be found in [31] or [32] for

example) seems a suitable way to derive temperatures from LIGS measurements for these higher enthalpy levels.

Another aspect is the limits imminent to the LIGS technique itself. For LIEGS (non-resonant LITA), a correlation of about p^2T^{-3} for the signal strength can be found in the literature [11,16,33]. For the resonant LITGS technique used in this work, the dependency of signal strength on pressure and temperature is predicted to be p^4T^{-6} for low densities and $p^{-2}T^{-0.6}$ for high densities [33]. However, in [33] only pressures up to 0.13 MPa were investigated, and it is stated that the downward trend of p^{-2} is expected to reduce at much higher pressures. This is consistent with successful LITGS measurements performed at a pressure level of 14 MPa reported in the literature [12].

A third point regarded increasingly relevant for higher enthalpies is non-equilibrium test gas conditions behind the reflected shock. In order to analyze a possible impact of the vibrational relaxation, the relaxation time was calculated according to [34] for the presented test runs taking into account the pressure and the temperature in the measurement volume prevailing at the time of measurement. For the measurements in shock tube mode (test runs M3 to M6), the calculated vibrational relaxation times are between 26 and 80 μ s. The measurements M4 to M6 were conducted 70 μ s after the reflected shock passed the measurement volume and thus at the later end of estimated relaxation time. Since the overall excitation of vibrational states at the comparatively low temperatures occurring here is rather small, the influence of vibrational relaxation is deemed negligible for these measurements. Note that due to variations in shock speed the LITGS measurement of test run M3 coincided with the reflected shock. Nevertheless, the measured pressure p_{meas} is nearly the same as for test run M4. The fact that the optically measured temperatures T_{LITGS} of both measurements (M3 and M4) only differ by a few Kelvin supports the assumption that vibrational relaxation has no considerable effect on the measurement data. The temperatures occurring during the runs M1 and M2 were too low for excitation of a vibrational state.

For the test runs at higher shock speeds, V1 and V2, the LITGS measurements were conducted approximately 60 μ s after the reflected shock passed the measurement volume. The calculated vibrational relaxation time for these conditions is only between 4 and 18 μ s, meaning that for these measurements no effect of the vibrational relaxation had to be taken into account. It was found that for higher temperatures, these values would even decrease. Therefore, at least from a vibrational point of view, no problems with non-equilibrium conditions are expected for LITGS temperature measurements in the near higher enthalpy range.

As a last possible limitation of LITGS in terms of high-enthalpy measurements, the absorbance of the seeding shall be briefly addressed: In general, in the test gas molecules

the population of energy levels changes with temperature. If a single absorption feature of the probed gas is based on a ground state, whose population decreases significantly for higher temperatures, the absorbance of the gas for the corresponding wavelength will decrease as well. In this work, NO₂ is used as the absorbing gas. Instead of a collection of single absorption features like diatomic molecules have, NO₂ has one broadband of overlapping absorption from 250 to 650 nm [29]. Due to the high overlap of several different transitions in the considered wavelength range, it is expected that the absorption of NO₂ does not decrease for higher temperatures, especially under high-pressure conditions, when pressure broadening even intensifies the overlapping of absorption features.

5 Conclusion

This work described the development of a LIGS measurement system for time-resolved, non-intrusive temperature measurements in the shock tunnel HELM. By adapting the optical setup of the system to the restrictions of the measurement task and by working with a minor seeding of NO, successful temperature measurements in the nozzle reservoir of a free-piston shock tunnel were realized. To the knowledge of the authors, this was the first time that optical temperature measurements were taken in this part of a shock tunnel.

For the shock tube mode, six successful measurements for a shock Mach number of about 2.35 were taken in total, two of them behind the incoming shock ($p \approx 1$ MPa, $T \approx 600$ K) and four after the passing of the reflected shock ($p \approx 4$ MPa, $T \approx 1000$ K). Apart from one outlier, the temperatures derived from LITGS signals were within a deviation range of 6% to a reference value calculated from the measured shock speed. The estimated uncertainty was less than or equal to 3.5% for all six measurements in the shock tube mode. Two LITGS signals from measurements behind the reflected shock in the shock tunnel mode were analyzed in detail. One of the signals allowed an unambiguous derivation of the temperature under the conditions of a shock with Mach 2.7 ($p \approx 5$ MPa, $T \approx 1200$ K, deviation 0.5%, uncertainty 4.9%).

The results in shock tunnel mode showed that the technique has the potential for successful measurements at higher temperatures as well, but needs to be enhanced for measurements at higher temperatures and for a limitation of effort (i.e., number of shock tunnel tests per successful LITGS measurement). When the conditions in the shock tunnel are increased in terms of temperatures and pressures in the near future, it is expected the seeding can be minimized or completely omitted due to NO₂ formation in the hot gas.

The possibility of reliable temperature measurements in the nozzle reservoir of the shock tunnel will not only help to enhance shock tunnel facilities but will also allow improve-

ments of numerical simulation tools. Furthermore, after the feasibility of LIGS measurements under very harsh and restricted conditions has been proven, new measuring tasks perhaps can be identified, where the LIGS technique can support difficult investigations on other unsolved problems and phenomena.

References

- Schemperg, K., Mundt, C.: Study of numerical simulations for optimized operation of the free piston shock tunnel HELM. In: 15th AIAA International Space Planes and Hypersonic Systems and Technologies Conference, AIAA Paper 2008-2653 (2008). <https://doi.org/10.2514/6.2008-2653>
- Stalker, R.J., Paull, A., Mee, D.J., Morgan, R.G., Jacobs, P.A.: Scramjets and shock tunnels—the Queensland experience. *Prog. Aerosp. Sci.* **41**(6), 471–513 (2005). <https://doi.org/10.1016/j.paerosci.2005.08.002>
- Sander, T., Altenhöfer, P., Mundt, C.: Development of laser-induced grating spectroscopy for application in shock tunnels. *J. Thermophys. Heat Transf.* **28**(1), 27–31 (2014). <https://doi.org/10.2514/1.t4131>
- Sander, T., Altenhöfer, P., Mundt, C.: Temperature measurements in a shock tube using laser-induced grating spectroscopy. *J. Thermophys. Heat Transf.* **30**(1), 62–66 (2016). <https://doi.org/10.2514/1.t4556>
- Pearse, R., Gaydon, A.: *The Identification of Molecular Spectra*, 4th edn. Chapman and Hall, London (1976)
- Hsu, D.K., Monts, D.L., Zare, R.N.: *Spectral Atlas of Nitrogen Dioxide 5330 to 6480 Å*. Academic Press, New York (1978)
- Altenhöfer, P.: *Aufbau und Anwendung eines LIGS-Messsystems am Stoßwellenkanal HELM*. Ph.D. Thesis, Institute for Thermodynamics, University of Federal Armed Forces Munich, Neubiberg, Germany (2017)
- Stalker, R.J.: A study of the free-piston shock tunnel. *AIAA J.* **5**(12), 2160–265 (1967). <https://doi.org/10.2514/3.4402>
- Mizukaki, T., Matsuzawa, T.: Application of laser-induced thermal acoustics in air to measurement of shock-induced temperature changes. *Shock Waves* **19**(5), 361–369 (2009). <https://doi.org/10.1007/s00193-009-0218-6>
- Herring, G., Meyers, J., Hart, R.: Shock-strength determination with seeded and seedless laser methods. *Meas. Sci. Technol.* **20**(4), 045304 (2009). <https://doi.org/10.1088/0957-0233/20/4/045304>
- Förster, F., Baab, S., Lamanna, G., Weigand, B.: Temperature and velocity determination of shock-heated flows with non-resonant heterodyne laser-induced thermal acoustics. *Appl. Phys. B* **121**(3), 235–248 (2015). <https://doi.org/10.1007/s00340-015-6217-7>
- Cummings, E.B.: *Laser-induced thermal acoustics*. Ph.D. Thesis, California Institute of Technology, Pasadena, United States (1995)
- Latzel, H., Dreizler, A., Dreier, T., Heinze, J., Dillmann, M., Stricker, W., Lloyd, G.M., Ewart, P.: Thermal grating and broadband degenerate four-wave mixing spectroscopy of OH in high-pressure flames. *Appl. Phys. B* **67**(5), 667–673 (1998). <https://doi.org/10.1007/s003400050563>
- Stampanoni-Panariello, A.: *Laser-induced gratings in the gas phase: formation mechanisms and applications for diagnostics*. Ph.D. Thesis, Swiss Federal Institute of Technology ETH, Zurich, Switzerland (2003). <https://doi.org/10.3929/ethz-a-004551741>
- Butenhoff, T.J.: Measurement of the thermal diffusivity and speed of sound of hydrothermal solutions via the laser-induced grating technique. *Int. J. Thermophys.* **16**(1), 1–9 (1995). <https://doi.org/10.1007/BF01438952>
- Schlamp, S., Rösgen, T., Kozlov, D., Rakut, C., Kasal, P., von Wolfersdorf, J.: Transient grating spectroscopy in a hot turbulent compressible free jet. *J. Propuls. Power* **21**(6), 1008–1018 (2005). <https://doi.org/10.2514/1.13794>
- Cummings, E.B.: Laser-induced thermal acoustics: simple accurate gas measurements. *Opt. Lett.* **19**(17), 1361–1363 (1994). <https://doi.org/10.1364/ol.19.001361>
- Stampanoni-Panariello, A., Kozlov, D.N., Radi, P.P., Hemmerling, B.: Gas phase diagnostics by laser-induced gratings. I. Theory. *Appl. Phys. B* **81**(1), 101–111 (2005). <https://doi.org/10.1007/s00340-005-1852-z>
- Stampanoni-Panariello, A., Kozlov, D.N., Radi, P.P., Hemmerling, B.: Gas phase diagnostics by laser-induced gratings. II. Experiments. *Appl. Phys. B* **81**(1), 113–129 (2005). <https://doi.org/10.1007/s00340-005-1853-y>
- Schlamp, S., Allen-Bradley, E.: Homodyne detection laser-induced thermal acoustics velocimetry. In: 38th Aerospace Sciences Meeting and Exhibit, AIAA Paper 2000-376 (2000). <https://doi.org/10.2514/6.2000-376>
- Cummings, E.B., Leyva, I.A., Hornung, H.G.: Laser-induced thermal acoustics (LITA) signals from finite beams. *Appl. Opt.* **34**(18), 3290–3302 (1995). <https://doi.org/10.1364/ao.34.003290>
- Lemmon, E., Jacobsen, R., Penoncello, S., Friend, D.: Thermodynamic properties of air and mixtures of nitrogen, argon, and oxygen from 60 to 2000 K at pressures to 2000 MPa. *J. Phys. Chem. Ref. Data* **29**(3), 331–385 (2000). <https://doi.org/10.1063/1.1285884>
- MATLAB and Curve Fitting Toolbox Release: The MathWorks Inc., Natick (2014)
- Oertel, H.: *Stoßrohre: Theorie, Praxis, Anwendungen; mit einer Einführung in die Physik der Gase*. Springer, Vienna (1966)
- Sander, T.: *Optische Messmethoden in der Aerothermodynamik/Thermofluidodynamik*. Habilitation, Institute for Thermodynamics, University of Federal Armed Forces Munich, Neubiberg (2016)
- Farooq, A., Jeffries, J.B., Hanson, R.K.: Sensitive detection of temperature behind reflected shock waves using wavelength modulation spectroscopy of CO₂ near 2.7 μm. *Appl. Phys. B* **96**(1), 161–173 (2009). <https://doi.org/10.1007/s00340-009-3446-7>
- Coleman, H., Steele, W.: *Experimentation and Uncertainty Analysis for Engineers*, 2nd edn. Wiley, New York (1989)
- Vandaele, A.C., Hermans, C., Simon, P.C., Carleer, M., Colin, R., Fally, S., Mérienne, M.F., Jenouvrier, A., Coquart, B.: Measurements of the NO₂ absorption cross-section from 42000 cm⁻¹ to 10000 cm⁻¹ (238–1000 nm) at 220 K and 294 K. *J. Quant. Spectrosc. Radiat. Transf.* **59**(3–5), 171–184 (1998). [https://doi.org/10.1016/S0022-4073\(97\)00168-4](https://doi.org/10.1016/S0022-4073(97)00168-4)
- Schneider, W., Moortgat, G.K., Tyndall, G.S., Burrows, J.P.: Absorption cross-sections of NO₂ in the UV and visible region (200–700 nm) at 298 K. *J. Photochem. Photobiol. A Chem.* **40**(2–3), 195–217 (1987). [https://doi.org/10.1016/1010-6030\(87\)85001-3](https://doi.org/10.1016/1010-6030(87)85001-3)
- Selcan, C., Sander, T., Altenhöfer, P., Koroll, F., Mundt, C.: Stagnation temperature measurements in a shock-tunnel facility using laser-induced grating spectroscopy. *J. Thermophys. Heat Transf.* **32**(1), 226–236 (2017). <https://doi.org/10.2514/1.T5199>
- Brown, M.S., Roberts, W.L.: Single-point thermometry in high-pressure, sooting, premixed combustion environments. *J. Propuls. Power* **15**(1), 119–127 (1999). <https://doi.org/10.2514/2.5400>
- Zuckerwar, A.: Speed of sound in real gases. I. Theory. *J. Acoust. Soc. Am.* **100**(4), 2747 (1996). <https://doi.org/10.1121/1.416879>
- Danehy, P.M., Paul, P.H., Farrow, R.L.: Thermal-grating contributions to degenerate four-wave mixing in nitric oxide. *J. Opt. Soc. Am. B Opt. Phys.* **12**(9), 1564–1576 (1995). <https://doi.org/10.1364/JOSAB.12.001564>
- Vincenti, W.G., Kruger, C.H.: *Introduction to Physical Gas Dynamics*. Robert E. Krieger Publishing Company, New York (1977)